

Modeling slow deformation of polygonal particles using DEM

Andrés A. Peña^a, Pedro G. Lind^{a,*}, Hans J. Herrmann^{b,c}

^a*Institute for Computational Physics, Universität Stuttgart,
Pfaffenwaldring 27, D-70569 Stuttgart, Germany,*

^b*Computational Physics, IfB, HIF E12, ETH Hönggerberg, CH-8093 Zürich, Switzerland,*

^c*Departamento de Física, Universidade Federal do Ceará,
60451-970 Fortaleza, Ceará, Brazil.*

Abstract

We introduce two improvements in the numerical scheme to simulate collision and slow shearing of irregular particles. First, we propose an alternative approach based on simple relations to compute the frictional contact forces. The approach improves efficiency and accuracy of the Discrete Element Method (DEM) when modeling the dynamics of the granular packing. We determine the proper upper limit for the integration step in the standard numerical scheme using a wide range of material parameters. To this end, we study the kinetic energy decay in a stress controlled test between two particles. Second, we show that the usual way of defining the contact plane between two polygonal particles is, in general, not unique which leads to discontinuities in the direction of the contact plane while particles move. To solve this drawback, we introduce an accurate definition for the contact plane based on the shape of the overlap area between touching particles, which evolves continuously in time.

Key words: Granular media, Discrete Element Method, Slow deformation, Contact forces.
PACS: 83.10.-y, 45.70.-n, 45.70.Cc, 02.60.-x

1 Motivation and model

To model the dynamics of granular media a commonly used approach is the well-known Discrete Element Method (DEM) [1–3]. When applied to slow shearing [4–6] the computation of frictional and therefore contact forces between particles may

* Corresponding author

Email address: lind@icp.uni-stuttgart.de (Pedro G. Lind).

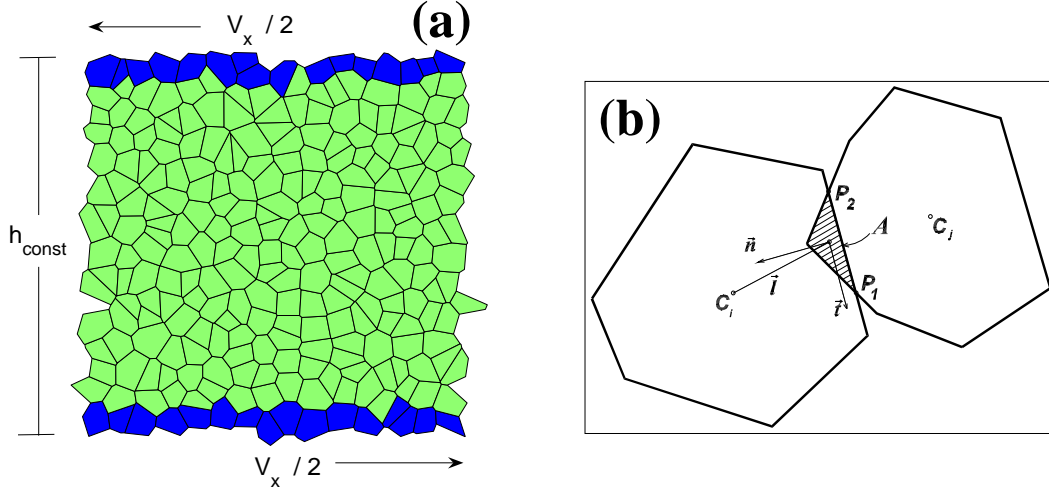


Fig. 1. **(a)** Sketch of the system of 256 particles (green particles) under shearing of top and bottom boundaries (blue particles). Horizontally periodic boundary conditions are considered and a constant low shear rate is chosen. **(b)** Illustration of two overlapping particles, where the overlap region A between particles fully characterizes the contact force \vec{F}^c .

introduce numerical errors that can be larger than the precision of the integration scheme used in DEM [7]. Moreover, if irregular particles are considered – typically polygons – the definition of the contact plane between touching particles is not straightforward.

In this paper we propose an approach to compute the tangential contact force with the same numerical precision as the normal force. Our improved procedure is specially suited for the case of slow shearing when large integration steps are needed for efficient computation, when studying e.g. the occurrence of avalanches [10] and the emergence of ratcheting in cyclic loading [11]. In addition, we discuss the drawbacks of the common procedures for computing the contact plane between touching particles. We will show that for polygonal (anisotropic) particles it varies discontinuously in time perturbing the proper convergence to the stationary state in stress controlled tests. To overcome this shortcoming we introduce a proper definition which does not depend on the shape of the touching particles and is suited for both regular and irregular particles.

Our model considers a two-dimensional system, as sketched in Fig. 1a. Each particle has two linear and one rotational degree of freedom, being contained between two boundary plates shearing against each other [8, 10, 19]. The volumetric strain is suppressed, i.e. the position of the walls is fixed and there is no dilation. Periodic boundary conditions are imposed in the horizontal direction. The evolution of the system is given by the integration of Newton’s equations of motion, where the resulting forces and momenta acting on each particle are given by the sum of all contact forces and torques applied on that particle, respectively. The boundary particles move with a fixed shear rate.

The integration of Newton's equation of motion is usually done with a predictor-corrector scheme [1, 12], which consists of three main stages, namely prediction, evaluation and correction. In the prediction stage one extracts for each particle the predicted position and acceleration of the center of mass. This is done by means of Taylor expansions of the linear and angular positions, yielding the corresponding velocities and higher-order time derivatives, as functions of the current values [12, 14]. During the evaluation stage, the predicted coordinate of each particle is used to determine the contact force $\vec{F}_{t+\Delta t}^c$ at time $t + \Delta t$. Since the method is not exact, there is a difference between the acceleration $\ddot{\vec{r}}(t + \Delta t) = \vec{F}_{t+\Delta t}^c/m$ and the value obtained in the prediction stage, namely $\Delta\ddot{\vec{r}} = \ddot{\vec{r}}(t + \Delta t) - \ddot{\vec{r}}^p(t + \Delta t)$. Finally, the difference $\Delta\ddot{\vec{r}}$ is used in the corrector step to correct the predicted position and its time derivatives, using proper weights for each time derivative [12]. The weights depend upon the order of the algorithm and the differential equation being solved. These corrected values are used for the next integration step $t + \Delta t$.

In our simulations we integrate equations of the form $\ddot{\vec{r}} = f(\vec{r}, \dot{\vec{r}})$, using a fifth order predictor-corrector algorithm that has a numerical error proportional to $(\Delta t)^6$ for each integration step [12].

Typically, the particles can neither break nor deform, i.e. fragmentation is neglected. The deformation is usually modeled by letting particles overlap [1, 15], as illustrated in Fig. 1b. The overlap between each pair of particles is considered to fully characterize the contact: the normal contact force is assumed to be proportional to the overlap area [19] and its direction perpendicular to the contact plane, which is usually defined by the intersection points between the boundaries of the two particles [19].

The contact forces, \vec{F}^c , are decomposed into their elastic and viscous contributions, \vec{F}^e and \vec{F}^v respectively. The elastic part of the contact force is simply given by the sum of the normal and the tangential components, with respect to the contact plane, namely

$$\vec{F}^e = F_n^e \hat{n}^c + F_t^e \hat{t}^c, \quad (1)$$

where the normal component reads

$$F_n^e = -k_n A/l_c, \quad (2)$$

with k_n the normal stiffness, A the overlap area and l_c the characteristic length of the contact, which, for two particles i and j , is given by $l_c = r_i + r_j$ with $r_i = \sqrt{A_i/2\pi}$ and A_i the area of the particle i , and similarly for particle j . The tangential force is considered to be proportional to the elastic elongation ξ of an imaginary spring – also called Cundall-Stack spring [15] – at the contact, namely

$$F_t^e = -k_t \xi, \quad (3)$$

where k_t is the tangential stiffness and ξ is the elastic elongation updated as

$$\xi(t + \Delta t) = \xi(t) + \vec{v}_t^c \Delta t, \quad (4)$$

where Δt is the time step of the DEM simulation, and \vec{v}_t^c is the tangential component of the relative velocity \vec{v}^c at the contact point.

Having both components of the elastic force, the tangential elastic elongation ξ is updated according to the Coulomb limit condition $|F_e^t| = \mu F_e^n$, with μ the interparticle friction coefficient. If the Coulomb condition is reached, particles are in the inelastic regime, and sliding is enforced by keeping constant the tangential force F_e^t . Here the tangential elongation ξ takes its maximum value $\pm \mu k_n A / (k_t l_c)$. Otherwise, if the contact is in the elastic regime ($|F_e^t| < \mu F_e^n$) the elongation ξ can increase in time, following Eq. (4).

The viscous force \vec{F}^v takes into account the dissipation at the contact which is important to maintain the numerical stability of the method. This force is calculated as [15]

$$\vec{F}^v = -m_r \nu \vec{v}^c, \quad (5)$$

where m_r is the reduced mass of the two touching particles and ν is the damping coefficient.

The suitable parameters for using this model are the interparticle friction μ , the normal stiffness k_n , the ratio k_t/k_n between tangential and normal stiffnesses and the ratio ϵ_t/ϵ_n between tangential and normal restitution coefficients. The restitution coefficients are defined from the contact stiffness and damping coefficient [16] as [17]

$$\epsilon_n = \exp(-\pi\eta/\omega) = \exp\left(-\frac{\pi}{\sqrt{4m_r k_n / \nu_n^2 - 1}}\right) \quad (6)$$

for the normal component, where $\omega = \sqrt{\omega_0^2 - \eta^2}$ is the frequency of the damped oscillator, with $\omega_0 = \sqrt{k_n/m_r}$ the frequency of the elastic oscillator, m_r the reduced mass, and $\eta = \nu_n/(2m_r)$ is the effective viscosity.

We start in Sec. 2 by describing the dependence of the above numerical procedure on the integration step, showing that the computation of the frictional forces yields a numerical error larger than the rest of the calculation. To overcome this shortcoming we then describe in Sec. 3 a geometrical improvement whose associated error is, for any studied case, of the same order as the error of the predictor-corrector scheme. In Sec. 4 we address the particular case of irregular particles, discussing the most common ways of computing the contact plane between touching particles and proposing a more suitable definition. Discussions and conclusions are given in

Sec. 5.

2 Choosing a proper integration step

The entire algorithm above relies on a proper choice of the integration step Δt , which should neither be too large to avoid divergence of the integration nor too small avoiding unreasonably long computational time. In this section we explore the numerical error introduced by the frictional force in Eq. (4) and determine the range of proper integration steps that guarantee convergence of the numerical scheme.

A typical criterion to choose the integration step Δt is to take a value such that $\Delta t < t_c/5$ [17, 18], where t_c is the characteristic duration of a contact defined by [5, 13, 17],

$$t_c = \frac{\pi}{\sqrt{\omega_0^2 - \eta^2}}. \quad (7)$$

While in several cases, one uses an integration step much smaller than the thresholds above [5], for low shear rate, very small integration steps imply a high computational effort, and so Δt should be chosen close to the threshold $t_c/5$. As shown below, the upper threshold (fraction of t_c) below which the numerical scheme converges, strongly depends on (i) the accuracy of the approach used to calculate frictional forces between particles, (ii) on the corresponding duration of the contact and (iii) on the number of degrees of freedom.

In a previous work [7] we have shown that considering values of Δt close to the upper limit $t_c/5$ yields relaxation times depending on Δt for the kinetic energy $E_k(i) = \frac{1}{2} (m_i \dot{r}_i^2 + I_i \vec{\omega}_i^2)$ of each particle i , when particles are subject to a non-zero friction. In particular, in the absence of friction ΔE_k attains a stationary value, while when friction is present it changes monotonically.

To obtain the proper threshold as function of the parameters of our model, we consider the simple situation of two circular particles in contact, as sketched in Fig. 2, and study the kinetic energy of one of them under external forcing. We start with two touching discs, say i and j , where i remains fixed and j is subject to a force \vec{F} perpendicular to its surface (no external torque is induced) along the x -axis. As a result of this external force, the disc j undergoes translation and rotation. The contact forces are obtained from the corresponding springs that are computed as described in Sec. 1 and act against the external force. This results in an oscillation of disc j till relaxation (dashed circle in Fig. 2) with a final center of mass displacement of ΔR and a rotation around the center of mass of $\Delta \theta$.

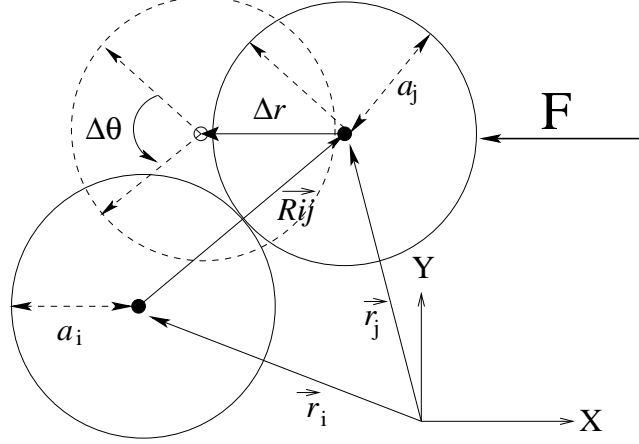


Fig. 2. Sketch of the stress controlled test of two particles (discs). The particle located at R_i remains fixed, while the particle at R_j is initially touching particle i . The vector \vec{R}_{ij} connecting the center of mass of particles i and j is initially oriented 45° with respect to the x -axis. After applying the constant force \vec{F} to disc j , the system relaxes till it reaches a new position (dashed circumference). Between its initial and final position particle j undergoes a displacement ΔR and a rotation $\Delta\theta$ (see text).

Since \vec{F} is kept constant, the procedure is stress controlled. Plotting the kinetic energy as a function of time, yields an exponential decay as

$$E_k(t) = E_k^{(0)} \exp\left(-\frac{t}{t_R(\Delta t)}\right), \quad (8)$$

where t_R is a relaxation time whose value clearly depends on the integration step Δt . Typically [7] the relaxation time t_R depends on Δt for integration steps larger than a given threshold $T_t t_c$. We define this threshold as the proper upper limit for the suitable integration steps. In other words, we want to determine the upper bound

$$\Delta t \lesssim T_t(\mu, k_t/k_n, \epsilon_t/\epsilon_n)t_c, \quad (9)$$

where $T_t(\mu, k_t/k_n, \epsilon_t/\epsilon_n)$ is a specific function that will be determined below.

We start by studying the influence of the stiffness, fixing $\mu = 500$ and $\epsilon_t/\epsilon_n = 1.0053$. Figure 3a shows the relaxation time t_R of the kinetic energy of the two-particle system for $k_n = 1, 50, 200, 10^4$ and 10^8 N/m. We see that decreasing Δt , the relaxation time t_R increases till it attains a maximum. This is due to the computation of the tangential force using the Cundall-spring scheme in Eq. (4) that yields smaller values for smaller integration steps. The stabilization of t_R occurs when Δt is small compared to the natural period $1/\omega_0$ of the system. Thus, T_t is the largest value of Δt for which we have this maximal relaxation time, in this case $T_t = 10^{-3}$. Further, all the curves in 3a can be collapsed by using the normalized integration step $\Delta t/t_c$, as shown in Fig. 3b. From the inset of Fig. 3b we also see that the contact time scales as $t_c \sim k_n^{-1/2}$, which comes from Eq. (7).

In the case where rotation is neglected, we obtain a constant $T_t = 10^{-4}$ as shown

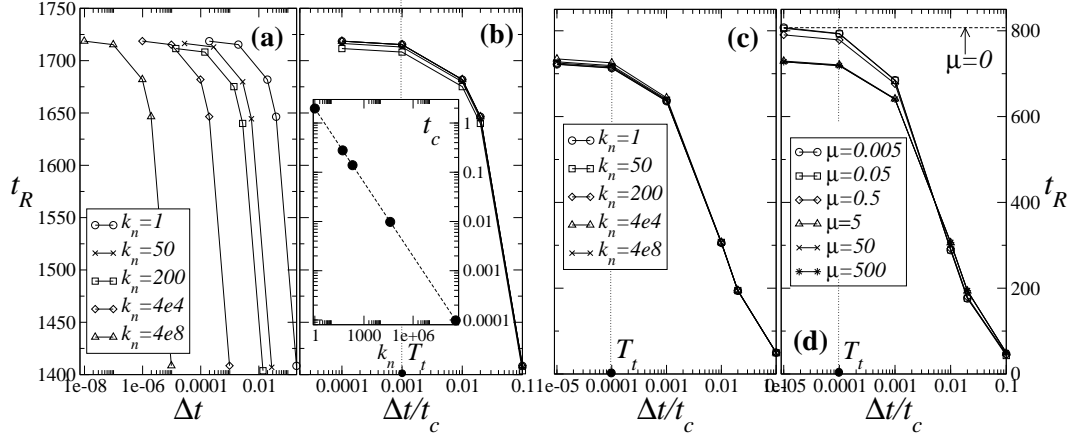


Fig. 3. The relaxation time t_R (in units of t_c) as a function of **(a)** the integration step Δt and **(b)** the normalized integration step $\Delta t/t_c$, where the contact time t_c is defined in Eq. (7). Here the friction coefficient is kept fixed $\mu = 500$ and different stiffnesses k_n (in units of N/m) are considered. The quotient $\Delta t/t_c$ collapses all the curves for different k_n . We find $t_c \sim k_n^{-1/2}$ as illustrated in the inset (see Eq. (7)). As a final result one finds a constant $T_t = 10^{-3}$. For other values of the friction coefficient one observes similar results. The relaxation time is also plotted as a function of the normalized integration step $\Delta t/t_c$, when rotation is suppressed. **(c)** $\mu = 500$ and different values of k_n and for **(d)** $k_n = 4 \times 10^8$ and different values of μ . The dashed horizontal line in (b) indicates the relaxation time of the kinetic energy in the absence of friction (see text).

in Fig. 3c. This T_t value is one order of magnitude smaller than the previous one in Eq. (9) and can be explained by considering an ‘infinite’ friction coefficient in the rotational degree of freedom [7]. Indeed, by comparing Fig. 3c with Fig. 3a, we see that the relaxation time t_R is smaller when rotation is suppressed. However, while

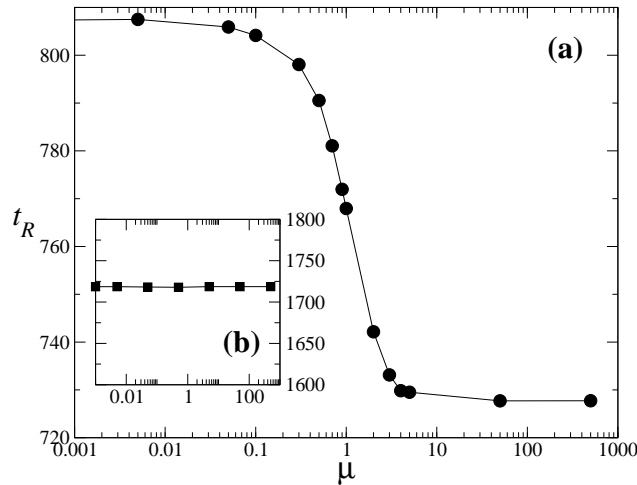


Fig. 4. The relaxation time t_R (in units of t_c) as a function of the friction coefficient μ **(a)** when rotation is suppressed and **(b)** when rotation is considered. Here, $k_n = 4 \times 10^8$ N/m which corresponds to a contact time $t_c = 9.8 \times 10^{-5}$ s. The normalized integration step $\Delta t/t_c = 10^{-5}$.

Fig. 3c clearly shows that t_R does not depend on the stiffness k_n , the same is not true for the friction coefficient μ , as shown in Fig. 3d.

In Fig. 4a we observe that, in the absence of rotation, there is a change of the relaxation time around $\mu = 1$, which is not observed when rotation is considered (Fig. 4b). This transition occurs since for larger values of $\mu > 1$, one has $F_t > F_n$, and therefore the frictional force increases and drives the system to relax faster. Further, with rotation one observes a larger t_R because there is an additional degree of freedom, that also relaxes.

We also check the dependence of the relaxation time on the two other parameters k_t/k_n and ϵ_t/ϵ_n . Figure 5a shows the relaxation time as a function of the normalized integration step $\Delta t/t_c$, using different stiffness ratios and with fixed $\mu = 500$ and ϵ_t/ϵ_n . We point out the following. First the convergence to a stationary value of t_R is faster for large stiffness ratio as $k_t/k_n \rightarrow 1$, yielding larger values of T_t . Second, the stationary value of t_R decreases with the stiffness ratios. This decrease is logarithmic, as shown in Fig. 5b.

The dependence of t_R on the stiffness ratio can be explained by taking into account that the larger the ratio k_t/k_n the larger F_t . Since the tangential force F_t controls the convergence of the numerical method, the larger k_t/k_n the faster the dissipation and

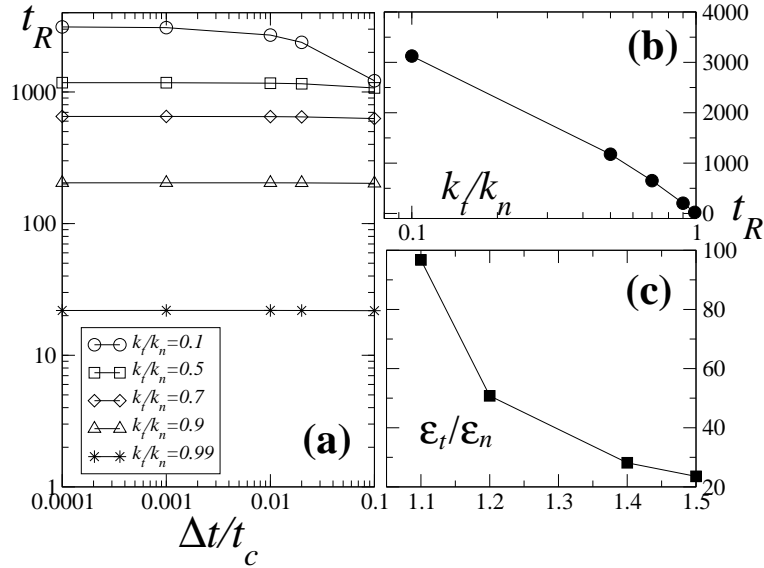


Fig. 5. Dependence of the relaxation time on the ratio k_t/k_n of the tangential and normal stiffnesses. **(a)** the convergence towards the relaxation time for decreasing integration steps using different stiffness ratio. **(b)** the approximate logarithmic dependence of t_R on k_t/k_n (see text). Here $\mu = 500$ and $\epsilon_t/\epsilon_n = 1.0053$. No rotational constraint is here considered. Dependence of the relaxation time on the ratio ϵ_t/ϵ_n of the tangential and normal restitution coefficients. **(a)** the convergence towards the relaxation time for decreasing integration steps using different restitution ratios. **(b)** the relaxation time t_R as a function of k_t/k_n (see text). Here $\mu = 500$ and $k_t/k_n = 1/3$. No rotational constraint is here considered.

thus, the smaller the stationary value of t_R . The logarithmic dependence observed in Fig. 5b can be explained from direct inspection of Eq. (6).

Figure 5c, showing the relaxation time as a function of the ratio ϵ_t/ϵ_n for fixed $\mu = 500$ and $k_t/k_n = 1/3$ can be explained similarly as in Fig. 5b. Here the dependence of the stationary value of t_R on ϵ_t/ϵ_n is approximately exponential.

When the Coulomb condition is fulfilled (inelastic regime), the dependence on Δt observed in all figures above, does not occur, since the strength of the tangential force is given by $F_t = \mu F_n$. All the previous results are taken within the elastic regime. This indicates that the improvements in the algorithm should be implemented when computing the elastic component of the tangential contact force, in Eq. (4), as explained in the next Section.

3 Improving the integration of the contact force

Using the Cundall's spring [4], the relaxation time of the two particles only converges when Δt is a small fraction T_t of the contact time t_c . Such dependence results from Eq. (4), that includes Δt in the computation of the tangential force in our predictor scheme which has an error of $(\Delta t)^2$.

To overcome this shortcoming, we propose a different expression to compute the elastic tangential elongation ξ . It is based on geometric relations and does not use Δt . Our expression for ξ contains only the quantities computed in the predictor step, guaranteeing a precision for ξ of the same order as the one of the predictor-corrector scheme. We illustrate our approach with the simple system of two discs, as sketched in Fig. 2, and discuss further the more realistic case of polygonal particles.

In Fig. 2, the elastic elongation of the tangential spring results from the superposition of both translation and rotational degrees of freedom, $\xi_j = \xi_j^{(tr)} + \xi_j^{(rot)}$.

For the translational contribution, the elastic elongation ξ depends only on the relative position of the two particles. In this case we substitute Eq. (4) by the expression

$$\xi_j^{(tr)}(t + \Delta t) = \xi_j^{(tr)}(t) + \frac{a_i}{a_i + a_j} (\vec{R}_{ij}^p(t + \Delta t) - \vec{R}_{ij}^p(t)) \cdot \hat{t}^c, \quad (10)$$

where a_i and a_j are the radii of the discs i and j respectively, \vec{R}_{ij} is the vector joining both centers of mass and points in the direction $i \rightarrow j$ (see Fig. 2). Index p indicates quantities derived from the coordinates computed at the predictor step.

Considering only the rotational contribution (\vec{R}_{ij} constant), the elastic elongation ξ

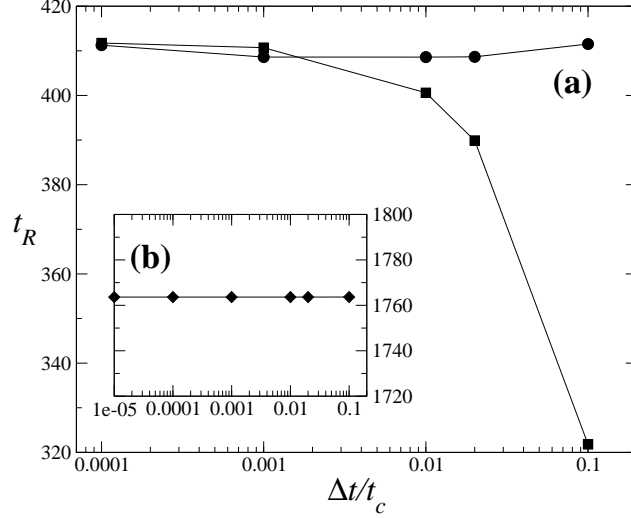


Fig. 6. **(a)** Comparison of the relaxation time t_R (in units of t_c) when using the standard integration scheme (squares) and the proposed improved scheme (circles). Here, we perform the stress control test between two particles with irregular polygonal shape, as illustrated in Fig. 1b and rotation is neglected (see text). **(b)** The relaxation time t_R (in units of t_c) using Eqs. (10) and (11) between two discs, as illustrated in Fig. 2; for the three cases when considering only rotation, only translation or both, the relaxation time remains constant independent of the integration step (see text).

depends only on rotation between times t and $t + \Delta t$:

$$\xi_j^{(rot)}(t + \Delta t) = \xi_j^{(rot)}(t) + (\theta_j^p(t + \Delta t) - \theta_j^p(t))a_j, \quad (11)$$

where $\theta_j^p(t)$ is the angle of some reference point on particle j at the predictor step of time t .

Using such expression, we have shown [7] that the relaxation time t_R is independent on the integration step. This is due to the fact that all quantities in the expressions above have an error of the same order of the predictor-corrector scheme.

When considering polygonal particles, one must also take into account the shape of the particles. For polygons, the decomposition of the elastic elongation ξ into translational and rotational contributions is not as trivial as for discs. This stems from the fact that the contact point no longer lies on the vector connecting the centers of mass. Thus, one should recalculate each time the position of the center of mass (only from translation) and the relative position of the vertices (only from rotation). For that, instead of using Eqs. (10) and (11), we compute the overlap areas between the two particles at times t and $t + \Delta t$ and consider the dislocation of the corresponding geometrical centers. This yields the translational contribution to the spring elongation. The contribution from the particle rotation is computed by determining the angular change due to the rotation of the branch vector between times t and $t + \Delta t$.

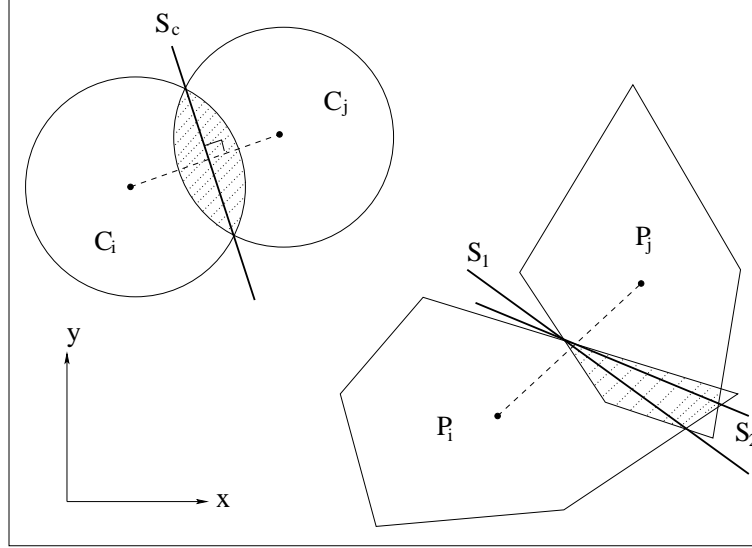


Fig. 7. Illustration of the definition of contact plane (thick solid lines) between touching discs and touching polygons. While for discs the definition is unique, since the plane S_c is perpendicular to the plain containing the center of the discs, for polygons the same is not true, yielding the possibility of more than one suitable choice.

Figure 6a compares how the relaxation time varies with the normalized time step when the standard Cundall approach is used (squares) and when our improved approach is introduced (circles). Clearly, the dependence on the integration step observed for the usual integration scheme disappears when our improved approach is introduced. Therefore, all the conclusions taken above for discs remain valid for polygons. In Fig. 6b we show the case of two discs for comparison.

4 An accurate definition of the contact plane

An additional improvement concerning polygons is the proper choice of the contact plane. Usually shear system consider the simple situation of spherical particles. Such particles yield a well defined contact plane, namely the vector perpendicular to the one connecting the centers of mass of the two touching particles. Figure 7 illustrates this definition of contact plane for the case of a two-dimensional system. In the case of polygons the branch vectors are not parallel and therefore no unique definition is possible. Usually [19] one usually chooses the plane containing the intersection points and of the boundaries of the two touching particles. When there are only two intersection points there is a unique possible contact plane. However, due to the motion of the particles, the overlap between them may give rise to more than two intersecting points that yields different possible contact planes. In Fig. 7 we illustrate a case where two different choices suit equally the condition above for a contact plane between two touching polygons.

In this Section, we propose to define the contact plane as the line passing through the center of mass of the overlap area having an orientation defined by an angle α_c (with the x -axis) given by the geometrical average of the orientation angles of each (non-oriented) edge of the overlap polygonal with respect to the x -axis. As shown below such definition is unique and guarantees a continuous variation of the orientation of the contact plane while the polygons move, as it is the case in a model of irregular particles under shearing.

More precisely, for an overlap polygon delimited by m edges, where each edge $n = 1, \dots, m$ lies on a specific line $y = x \tan \alpha_n + b_n$, the contact plane in the two-dimensional case is defined from

$$y = x \tan \alpha_c + b_c, \quad (12)$$

where $b_c = y_c - x_c \tan \alpha_c$ with (x_c, y_c) the coordinates of the center of mass of the overlap polygon, and

$$\alpha_c = \frac{\sum_{n=1}^m \alpha_n \ell_n}{\sum_{n=1}^m \ell_n}, \quad (13)$$

with ℓ_n the length of segment n . Since the angles α_n are angles between non-oriented lines, they can be acute or obtuse. To solve this indetermination we choose all the angles for the sum in Eq. (13) to be acute. Then, after computing α_c we choose either the line in Eq. (12) or the one perpendicular to it, depending which one is more perpendicular to the line joining the center of mass of both particles.

The main advantage of our definition in Eq. (13) is that while particles move the orientation of the contact plane varies continuously with their overlap (polygonal) area, as illustrated in Fig. 8 with the curve marked by bullets. On the contrary, contact planes taken from two intersection points of the two polygons present frequent discontinuities, as can be seen from the examples with squares in Fig. 8. Such discontinuities occur since not only the size and orientation of the edges defining the overlap polygon vary in time, but also the *number* of edges.

There is also the advantage that such a definition enables the system to behave as physically expected. For instance, during relaxation of a stress controlled test as illustrated in Fig. 9, the characteristic physical properties oscillate and converge to a stationary value. In Fig. 9 we plot both F_t/F_n and α_c for both definitions. We can see that the convergence of the new definition is similar to a damped oscillation, contrary to what is observed for the conventional definition. Such deviation from the damped oscillation behavior occurs due to the discontinuities observed in Fig. 8, which act as external excitations in the damping of the particles oscillation. As a consequence, the relaxation time associated with the discontinuous contact plane is smaller than when using our definition, as illustrated in Fig. 10.

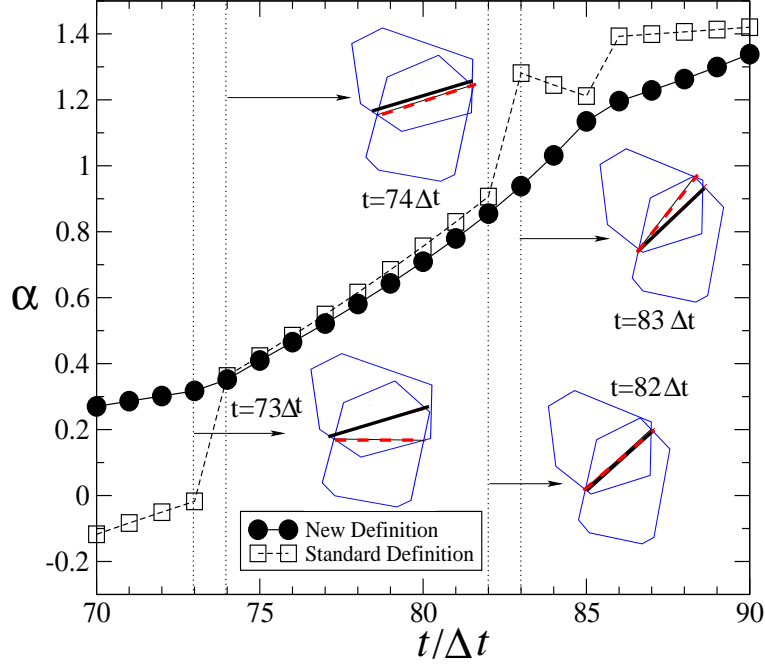


Fig. 8. Illustration of the orientation of the contact plane, given by angle α_c as a function of time when two polygons overlap each other. Two different definitions of contact plane are considered: the usual definition (squares) and the one proposed (bullets), as given in Eq. (13). One sees that while the proposed definition varies continuously, the usual definition shows discontinuities that influence the contact between touching polygons (see also Figs. 9 and 10).

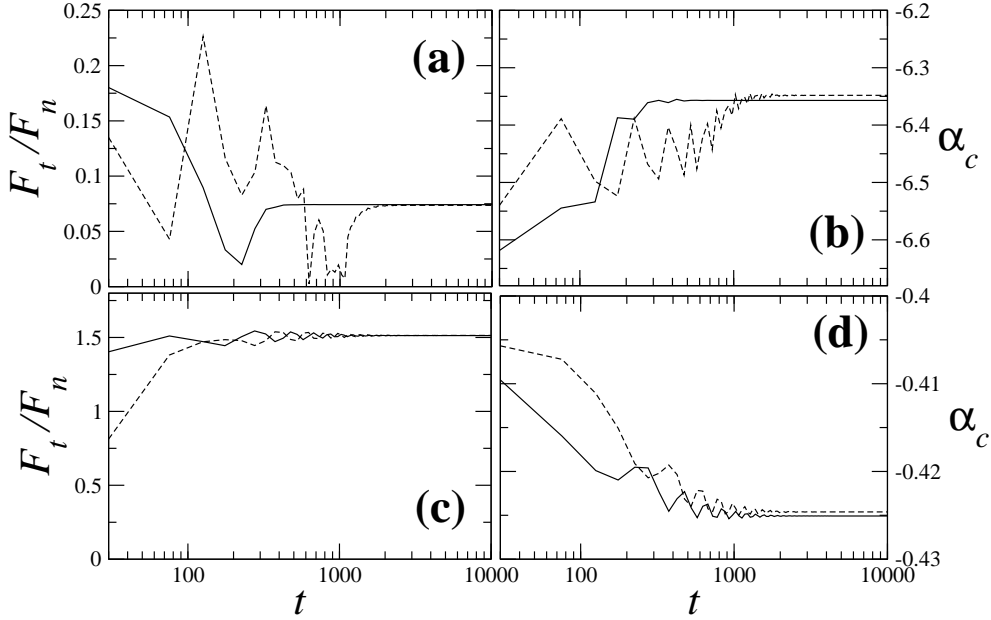


Fig. 9. Time evolution of (a) the ratio F_t/F_n and (b) of α_c for the usual definition of the contact plane. The same evolution is plotted for (c)-(d) the new definition in Eq. (13). In each case two curves are plotted, corresponding to two different integration steps (see text).

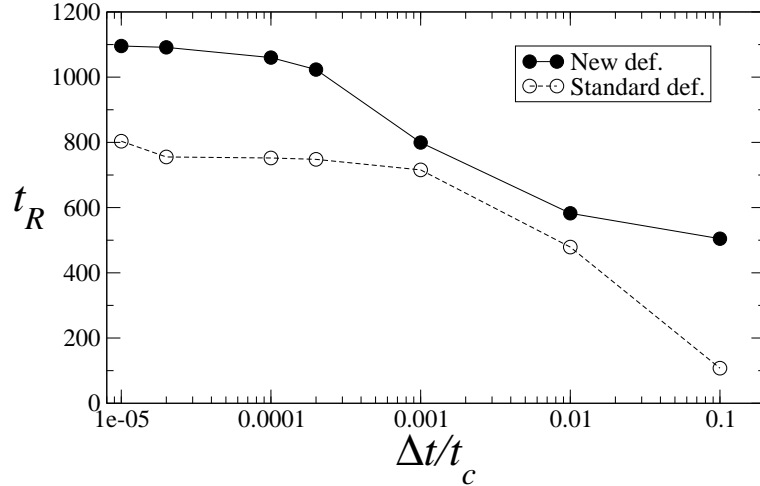


Fig. 10. The relaxation time as a function of the integration step for the usual definition (circles) and the new definition of the contact plane (bullets).

5 Discussion and conclusions

We introduced a technique to improve the accuracy of the numerical scheme used to compute the evolution of particle systems, showing that the range of admissible integration steps has an upper limit significantly smaller than previously assumed. The new approach for computing the frictional forces is an alternative to the Cundall spring, given by Eqs. (10) and (11) and suits not only the simple situation of discs but also more realistic ones, where particles have polygonal shape.

Further, our upper limit of the admissible range of integration steps was determined for a single contact using a stress controlled test. Its dependence on the stiffness, restitution coefficient and friction coefficient was carefully addressed. When a larger system (N particles) is studied, multiple contacts must be taken into account, which will yield an upper limit that we conjecture to be $1/N$ of the upper limit obtained above.

Finally, for the case of polygonal particles, we also introduced a definition for the contact plane between two touching particles. Our definition is not only based on the intersections points of the particles in contact but also on the geometry of the overlap area. Thus, the contact plane varies continuously during the stress controlled tests and is unique, contrary to the usual definition.

Acknowledgments

The authors thank Sean McNamara and Fernando Alonso-Marroquín for useful discussions. We thank support by German-Israeli Foundation and by *Deutsche*

Forschungsgemeinschaft, under the project HE 2732781. PGL thanks support by *Deutsche Forschungsgemeinschaft*, under the project LI 1599/1-1. HJH thanks the Max Planck prize.

References

- [1] T. Pöschel and T. Schwager, *Computational Granular Dynamics* (Springer, Berlin, 2005).
- [2] M.P. Ciamarra, A. Coniglio, M. Nicodemi, Phys. Rev. Lett. **94** 188001 (2005).
- [3] F. da Cruz, S. Eman, M. Prochnow, J.N. Roux Phys. Rev. E. **72** 021309 (2005).
- [4] P.A. Cundall, Ingenieur-Archiv **59**, 148 (1989).
- [5] P.A. Thompson, G.S. Grest, Phys. Rev. Lett. **67** 1751 (1991).
- [6] A.A. Peña, R. García-Rojo, H.J. Herrmann, Granular Matter, **9**:279-291 (2007).
- [7] A.A. Peña, P.G. Lind, S. McNamara and H. Herrmann, “Numerical improvement of the discrete element method applied to shear of granular media”, submitted, 2007.
- [8] F. Alonso-Marroquín, I. Vardoulakis, H.J. Herrmann, D. Weatherley, P. Mora, Phys. Rev. E **74**, 031306 (2006).
- [9] P. Mora, D. Place, Pageoph. **143**, 61 (1994).
- [10] P. Mora, D. Place, Geophys. Res. Lett. **26**, 123 (1999).
- [11] S. McNamara, R. García-Rojo and H.J. Herrmann, preprint 2007.
- [12] M.P. Allen and D.J. Tildesley, *Computer Simulation of Liquids* (Oxford Univ. Press, Oxford, 2003).
- [13] S. Luding, E. Clément, A. Blumen, J. Rajchenbach, J. Duran, Phys. Rev. E **50**, 4113 (1994).
- [14] E. Rougier, A. Munjiza, N.W.M. John, Int. J. Numer. Meth. Eng. **61**, 856 (2004).
- [15] P.A. Cundall and O.D.L. Strack, Géotechnique **29**, 47-65 (1979).
- [16] S.F. Foerster, M.Y. Louge, H. Chang, K. Allia, Phys. Fluids **6(3)**, 1108 (1994).
- [17] S. Luding, in *Physics of Dry Granular Media*, H.J. Herrmann, J.-P. Hovi, and S. Luding (Kluwer Academic Publishers, Dordrecht, 1998), pp. 285.
- [18] H.-G. Matuttis, Granular Matter **1**, 83 (1998).
- [19] H.J. Tillemans, H.J. Herrmann, Physica A **217**, :261-288 (1995).
- [20] F. Alonso-Marroquín and H.J. Herrmann, Phys. Rev. Lett. **92**, 054301 (2004).
- [21] S. Latham, S. Abe, P. Mora, in R. García-Rojo, H.J. Herrmann, and S. McNamara (eds.), *Powders and Grains 2005*, (Balkema, Stuttgart, 2005) pp. 213.